

## ***B*-hadron fragmentation functions at next-to-next-to-leading order from a global analysis of $e^+e^-$ annihilation data**

Maral Salajegheh,<sup>1,\*</sup> S. Mohammad Moosavi Nejad,<sup>1,3,†</sup> Hamzeh Khanpour,<sup>2,3,‡</sup>  
Bernd A. Kniehl,<sup>4,§</sup> and Maryam Soleymaninia<sup>3,||</sup>

<sup>1</sup>*Faculty of Physics, Yazd University, P.O. Box 89195-741, Yazd, Iran*

<sup>2</sup>*Department of Physics, University of Science and Technology of Mazandaran,  
P. O. Box 48518-78195, Behshahr, Iran*

<sup>3</sup>*School of Particles and Accelerators, Institute for Research in Fundamental Sciences (IPM),  
P.O. Box 19395-5531, Tehran, Iran*

<sup>4</sup>*II. Institut für Theoretische Physik, Universität Hamburg, Luruper Chaussee 149,  
22761 Hamburg, Germany*



(Received 18 April 2019; published 3 June 2019)

We present nonperturbative fragmentation functions (FFs) for bottom-flavored ( $B$ ) hadrons both at next-to-leading (NLO) and, for the first time, at next-to-next-to-leading order in the  $\overline{\text{MS}}$  factorization scheme with five massless quark flavors. They are determined by fitting all available experimental data of inclusive single  $B$ -hadron production in  $e^+e^-$  annihilation, from the ALEPH, DELPHI, and OPAL collaborations at CERN LEP1 and the SLD collaboration at SLAC SLC. The uncertainties in these FFs as well as in the corresponding observables are estimated using the Hessian approach. We perform comparisons with available NLO sets of  $B$ -hadron FFs. We apply our new FFs to generate theoretical predictions for the energy distribution of  $B$  hadrons produced through the decay of unpolarized or polarized top quarks, to be measured at the CERN LHC.

DOI: [10.1103/PhysRevD.99.114001](https://doi.org/10.1103/PhysRevD.99.114001)

### **I. INTRODUCTION**

For a long time, there has been considerable interest in the study of bottom-flavored-hadron ( $B$ -hadron) production at hadron and  $e^+e^-$  colliders, both experimentally and theoretically. Historically, the first measurements were performed more than 3 decades ago by the UA1 collaboration at the CERN  $Sp\bar{p}S$  collider [1] operating at center-of-mass (c.m.) energy  $\sqrt{s} = 630$  GeV.

In the framework of the parton model of QCD, the description of the inclusive single production of identified hadrons  $h$  involves fragmentation functions (FFs),  $D_a^h(x, Q^2)$ . At leading order, their values correspond to the probability that the colored parton  $a$ , which is produced at short distance, of order  $1/\sqrt{Q^2}$ , fragments into the colorless hadron  $h$  carrying the fraction  $x$  of the energy of

$a$ . Given their  $x$  dependence at some scale  $Q_0$ , the evolution of the FFs with  $Q^2$  may be computed perturbatively from the timelike Dokshitzer-Gribov-Lipatov-Altarelli-Parisi (DGLAP) equations [2–4]. The timelike splitting functions  $P_{a\rightarrow b}^T(x, \alpha_s(Q^2))$  appearing therein are known through next-to-next-to-leading order (NNLO) [5–7]. In the case of  $e^+e^-$  annihilation, the hard-scattering cross sections for the inclusive production of parton  $a$ , to be convoluted with  $D_a^h(x, Q^2)$ , are also known through NNLO [5,8–11]. This allows one to interpret  $e^+e^-$  data of the inclusive single production of hadron  $h$  at NNLO and thus to extract FFs at this order [12–15]. Owing to the factorization theorem, the FFs are independent of the process by which parton  $a$  is produced. This allows one to transfer experimental information from  $e^+e^-$  annihilation to any other production mechanism, such as photoproduction, leptonproduction, hadroproduction, and two-photon scattering. Of all these processes,  $e^+e^-$  annihilation provides the cleanest laboratory for the extraction of FFs, being devoid of nonperturbative effects beyond fragmentation itself. Presently, there is particular interest in hadroproduction at the BNL Relativistic Heavy Ion Collider (RHIC) and the CERN Large Hadron Collider (LHC) due to ongoing experiments.

The parton model of QCD implemented in the modified minimal-subtraction ( $\overline{\text{MS}}$ ) factorization scheme with  $n_f$

\*M.Salajegheh@stu.yazd.ac.ir

†Mmoosavi@yazd.ac.ir

‡Hamzeh.Khanpour@mail.ipm.ir

§kniehl@desy.de

||Maryam\_Soleymaninia@ipm.ir

*Published by the American Physical Society under the terms of the Creative Commons Attribution 4.0 International license. Further distribution of this work must maintain attribution to the author(s) and the published article's title, journal citation, and DOI. Funded by SCOAP<sup>3</sup>.*

massless-quark flavors, the so-called zero-mass variable-flavor-number scheme (ZM-VFNS), can also be applied to the open production of heavy flavors, such as  $D$  and  $B$  hadrons, provided the hard energy scale characteristic for the production process is sufficiently larger than the heavy-flavor mass. This is certainly the case for all the applications here, because  $M_B \ll M_Z, m_t$ . Recently,  $D$  hadron FFs have been provided at NNLO in Ref. [16]. Here, we perform the first NNLO determination of  $B$ -hadron FFs.

In Refs. [17,18],  $B$ -hadron FFs were extracted at NLO in the ZM-VFNS by fitting to the fractional-energy distributions  $d\sigma/dx_B$  of the cross section of  $e^+e^- \rightarrow B + X$  measured by the ALEPH [19] and OPAL [20] collaborations at the CERN Large Electron Positron Collider (LEP1) and the SLD collaboration [21] at the SLAC Linear Collider (SLC).

In the meantime, also the DELPHI collaboration has reported a similar measurement at LEP1 [22]. In the present work, these data are, for the first time, included in a  $B$ -hadron FF fit. On the other hand, we are not aware of any other such data from  $e^+e^-$  annihilation. In want of NNLO hard-scattering cross sections for inclusive single  $B$ -hadron production from other initial states, we do concentrate here on  $e^+e^-$  annihilation. We also go beyond Refs. [17,18] by performing a full-fledged error estimation, both for the FFs and the resulting differential cross sections, using the Hessian approach [23].

The LEP1 experiments [19,20,22] identified the  $B$  hadrons by their semileptonic decays,  $B \rightarrow D^{(*)}\ell\nu$ , while the SLD collaboration [21] collected an inclusive sample of reconstructed  $B$ -hadron decay vertices. The bulk of the experimentally observed  $B$  hadrons is made up by  $B^\pm$ ,  $B^0/\bar{B}^0$ , and  $B_s^0/\bar{B}_s^0$  mesons.

The outline of this paper is as follows: In Sec. II, we describe the theoretical framework of inclusive single hadron production in  $e^+e^-$  annihilation through NNLO in the ZM-VFNS and introduce our parametrization of the  $b/\bar{b} \rightarrow B$  FF at the initial scale. In Sec. III, we explain the minimization method in our analysis and our approach to error estimation. In Sec. IV, our NLO and NNLO results are presented and compared with the experimental data fitted to. In Sec. V, we present our NLO predictions for the normalized-energy distributions of  $B$  hadrons from decays of (un) polarized top quarks. Our conclusions are given in Sec. VI.

## II. QCD FRAMEWORK FOR $B$ -HADRON FFs

As mentioned in Sec. I, we fit nonperturbative  $B$ -hadron FFs to measured  $x_B$  distributions of the cross section of

$$e^+e^- \rightarrow (\gamma^*, Z) \rightarrow B + X, \quad (1)$$

where  $X$  refers to the unobserved part of the final state. In the following, we explain how to evaluate the cross section

of process (1) at NLO and NNLO in the ZM-VFNS. Denoting the four-momenta of the virtual gauge boson and the  $B$  hadron by  $q$  and  $p_B$ , respectively, we have  $s = q^2$ ,  $p_B^2 = m_B^2$ , and  $x_B = 2(p_B \cdot q)/q^2$ . In the c.m. frame,  $x_B = 2E_B/\sqrt{s}$  is the energy of the  $B$  hadron in units of the beam energy. In the ZM-VFNS, we have

$$\begin{aligned} & \frac{1}{\sigma_{\text{tot}}} \frac{d\sigma}{dx_B} (e^+e^- \rightarrow B + X) \\ &= \sum_i \int_{x_B}^1 \frac{dx_i}{x_i} \frac{1}{\sigma_{\text{tot}}} \frac{d\sigma_i}{dx_i} (x_i, \mu_R, \mu_F) D_i^B \left( \frac{x_B}{x_i}, \mu_F \right), \end{aligned} \quad (2)$$

where  $i = g, u, \bar{u}, \dots, b, \bar{b}$  runs over the active partons with four-momenta  $p_i$ ,  $d\sigma_i(x_i, \mu_R, \mu_F)/dx_i$  is the partonic cross section of  $e^+e^- \rightarrow i + X$  differential in  $x_i = 2(p_i \cdot q)/q^2$ ,  $D_i^B(z, \mu_F)$  is the  $i \rightarrow B$  FF, and  $\mu_R$  and  $\mu_F$  are the renormalization and factorization scales, respectively. The latter are *a priori* arbitrary, but a typical choice is  $\mu_F = \mu_R = \sqrt{s}$ . In the c.m. frame,  $z = x_B/x_i$  is the fraction of energy passed on from parton  $i$  to the  $B$  hadron. It is customary in experimental analyses to normalize Eq. (2) by the total hadronic cross section,

$$\sigma_{\text{tot}} = \frac{4\pi\alpha^2(s)}{s} \left( \sum_i^{n_f} \tilde{e}_i^2(s) \right) (1 + \alpha_s K_{\text{QCD}}^{(1)} + \alpha_s^2 K_{\text{QCD}}^{(2)} + \dots), \quad (3)$$

where  $\alpha$  and  $\alpha_s$  are the fine-structure and strong-coupling constants, respectively,  $\tilde{e}_i$  is the effective electroweak charge of quark  $i$ , and the coefficient  $K_{\text{QCD}}^{(n)}$  contains the  $N^n$ LO correction. Here, we need  $K_{\text{QCD}}^{(1)} = 3C_F/(4\pi)$ , with  $C_F = 4/3$ , and  $K_{\text{QCD}}^{(2)} \approx 1.411$  [24].

The  $z$  distribution of the  $b \rightarrow B$  FF at the starting scale  $\mu_0$  is a genuinely nonperturbative quantity to be extracted from experimental data. Its form is unknown, and an educated guess is in order. The selection criterion is to score a minimum  $\chi^2$  value as small as possible with a set of fit parameters as minimal as possible. As in Refs. [17,18], we adopt here the simple power ansatz [25],

$$D_b^B(z, \mu_0) = N_b z^{\alpha_b} (1-z)^{\beta_b}, \quad (4)$$

with fit parameters  $N_b$ ,  $\alpha_b$ , and  $\beta_b$ , and choose  $\mu_0 = m_b = 4.5$  GeV. This ansatz was found to enable excellent fits [17,18]. The  $i \rightarrow B$  FFs for the other quarks and the gluon are assumed to be zero at  $\mu_F = \mu_0$  and are generated through the DGLAP evolution to larger values of  $\mu_F$ . We take  $\alpha_s(M_Z)$  to be an input parameter and adopt the world average value 0.1181 for  $n_f = 5$  [26] both at NLO and NNLO.

As mentioned in Sec. I, we fit to ALEPH [19], DELPHI [22], OPAL [20], and SLD [21] data. These datasets reach down to very small  $x_B$  values, which fall outside the range of validity of our fixed-order approach. In fact, in the small- $x_B$  limit, both the timelike splitting functions and the hard-scattering cross sections develop soft-gluon logarithms that require resummation. At the same time, finite- $m_b$  and finite- $M_B$  effects become relevant there. We leave the implementation of these refinements for future work, and instead impose appropriate minimum- $x_B$  cuts for the time being. Specifically, we only include ALEPH data points with  $x_B \geq 0.25$ , DELPHI data points with  $x_B \geq 0.36$ , OPAL data points with  $x_B \geq 0.325$ , and SLD data points with  $x_B \geq 0.28$ . This enables acceptable fits within the fit range, at the expense of certain deviations in the small- $x_B$  range, of course. The fixed-order approach is also challenged in the large- $x_B$  limit, by the emergence of threshold logarithms, which also require resummation. In practice, however, these effects do not jeopardize the quality of our fits, so that we refrain from imposing maximum- $x_B$  cuts.

### III. DETERMINATION OF B-HADRON FFs AND THEIR UNCERTAINTIES

We now explain our fitting procedure. For a given set  $p = \{N_b, \alpha_b, \beta_b\}$  of fit parameters, the goodness of the overall description of the experimental data by the theoretical predictions is measured by the global  $\chi^2$  value,

$$\chi_{\text{global}}^2(p) = \sum_{n=1}^{N^{\text{exp}}} w_n \chi_n^2(p), \quad (5)$$

where  $n$  labels the  $N^{\text{exp}} = 4$  experimental datasets,  $w_n$  are their weight factors [27,28], which we take to be unity, and

$$\chi_n^2(p) = \left( \frac{1 - \mathcal{N}_n}{\Delta \mathcal{N}_n} \right)^2 + \sum_{i=1}^{N_n^{\text{data}}} \left( \frac{\mathcal{N}_n \mathcal{F}_{n,i}^{\text{exp}} - \mathcal{F}_{n,i}^{\text{theo}}(p)}{\mathcal{N}_n \Delta \mathcal{F}_{n,i}^{\text{exp}}} \right)^2 \quad (6)$$

is the  $\chi^2$  value of dataset  $n$ . On the experimental side,  $\mathcal{F}_{n,i}^{\text{exp}}$  is the central value of  $(1/\sigma_{\text{tot}})d\sigma/dx_B$  measured in bin  $i$  out of the  $N_n^{\text{data}}$  bins in dataset  $n$ ,  $\Delta \mathcal{F}_{n,i}^{\text{exp}}$  is its individual error obtained by combining statistical and systematic errors in quadrature,  $\mathcal{N}_n$  is the unknown overall normalization factor of dataset  $n$  to be fitted, and  $\Delta \mathcal{N}_n$  is its error as quoted by the experimental collaboration. On the theoretical side,  $\mathcal{F}_{n,i}^{\text{theo}}(p)$  is the respective NLO or NNLO prediction.

We determine the fit parameters  $p$  by minimizing Eq. (5) with the help of the Monte Carlo package MINUIT [29] from the CERN program library. We adopt a two-step procedure. In the prefitting stage, we determine the four values  $\mathcal{N}_n$  by fitting them simultaneously with the three fit parameters  $p$ . In the main fitting stage, we then refine the determination of  $p$  with large statistics keeping  $\mathcal{N}_n$  fixed. In the evaluation of  $\chi_{\text{global}}^2(p)/\text{DOF}$ , we take the number of degrees of

freedom (DOF) to be the overall number of data points fitted to minus three for the proper fit parameters  $p$ . We find the APFEL library [30] to be a very useful FF fitting tool.

We now describe our methodology for the estimation of the uncertainties in the  $B$ -hadron FFs. We adopt the Hessian approach to the propagation of uncertainties from the experimental datasets to the FFs, which has proven of value in global analyses of parton distribution functions and has been frequently applied there. For definiteness, we ignore additional sources of uncertainties, which are mostly of theoretical origin and are negligible against the experimental uncertainties taken into account here. In the following, we briefly review our procedure. For more details, we refer to Ref. [31].

In the Hessian approach, the uncertainty bands on the  $B$ -hadron FFs,  $\Delta D_b^B(z)$ , may be obtained through linear error propagation,

$$[\Delta D^B(z)]^2 = \Delta \chi_{\text{global}}^2(\hat{p}) \sum_{i,j} \frac{\partial \Delta D^B(z, \hat{p})}{\partial p_i} \times H_{ij}^{-1}(\hat{p}) \frac{\partial \Delta D^B(z, \hat{p})}{\partial p_j}, \quad (7)$$

where  $p_i$  ( $i = 1, 2, 3$ ) are the free parameters in Eq. (4),  $\hat{p}_i$  are their optimized values, and  $H^{-1}(p)$  is the covariance matrix, which is a default output of the MINUIT program [29]. In Eq. (7), we have suppressed the label  $\mu_F$  for the factorization scale, which we take to be  $\mu_0$ . The error bands  $\Delta D^B(z)$  are subject to DGLAP evolution in  $\mu_F$  along with the central values  $D^B(z)$ . The confidence level (C.L.) is controlled by  $T^2 = \Delta \chi_{\text{global}}^2$ . We adopt the standard parameter fitting criterion by choosing  $T = 1$ , which corresponds to the 68% C.L., i.e., the  $1\sigma$  error band. In Sec. IV, the uncertainty bands thus determined are presented both for the  $B$ -hadron FFs and for the physical observables evaluated with them.

### IV. RESULTS AND DISCUSSION

We are now in a position to present our results for the  $B$ -hadron FFs both at NLO and NNLO and to compare the resulting theoretical predictions with the experimental data fitted to, so as to check directly the consistency and goodness of our fits. We also compare our  $B$ -hadron FFs with the NLO ones presented by Kniehl, Kramer, Schienbein, and Spiesberger (KKSS) [18].

In Table I, for each of the four experimental datasets  $n$ , from ALEPH [19], DELPHI [22], OPAL [20], and SLD [21], the number  $N_n^{\text{data}}$  of data points included in the NLO and NNLO fits and the normalization factors  $\mathcal{N}_n$  and the  $\chi_n^2(p)$  values thus obtained are specified together with the total number of data points and the values of  $\chi_{\text{global}}^2(p)$  and  $\chi_{\text{global}}^2(p)/\text{DOF}$ . There are  $59 - 3 = 56$  degrees of freedom. The NLO and NNLO fits are both excellent, with

TABLE I. Numbers  $N_n^{\text{data}}$  of data points from dataset  $n$  included in the NLO and NNLO fits and normalization factors  $\mathcal{N}_n$  and  $\chi_n^2$  values thus obtained; total number of data points;  $\chi_{\text{global}}^2(p)$  values; and  $\chi_{\text{global}}^2(p)/\text{DOF}$  values.

Collaboration	$N_n^{\text{data}}$	$\mathcal{N}_n^{\text{NLO}}$	$\mathcal{N}_n^{\text{NNLO}}$	$\chi_n^{2,\text{NLO}}$	$\chi_n^{2,\text{NNLO}}$
ALEPH [19]	18	1.0008	1.0011	14.376	12.269
DELPHI [22]	8	0.9993	1.0058	7.535	15.377
OPAL [20]	15	0.9951	0.9958	35.594	20.002
SLD [21]	18	1.0030	0.9996	25.675	14.195
Total	59			83.180	61.844
$\chi_{\text{global}}^2(p)/\text{DOF}$				1.485	1.104

$\chi_{\text{global}}^2(p)/\text{DOF}$  values of order unity. As expected on general grounds,  $\chi_{\text{global}}^2(p)/\text{DOF}$  is reduced as one passes from NLO to NNLO. This is also true for the individual datasets, except for the most recent one, from DELPHI. The NLO and NNLO fit results for  $p$  are summarized in Table II.

In Fig. 1, the  $z$  distributions of the NLO and NNLO  $b \rightarrow B$  FFs at the initial scale  $\mu_F = \mu_0$  are compared with each other. The NLO and NNLO results agree in shape and position of maximum, but differ in normalization. This difference is induced by the  $\mathcal{O}(\alpha_s^2)$  correction terms in the hard-scattering cross sections and in the timelike splitting functions, and it is compensated in the physical cross sections to be compared with the experimental data up to terms beyond  $\mathcal{O}(\alpha_s^2)$ . The error bands determined as described in Sec. III are also shown in Fig. 1. They are dominated by the experimental errors, which explains why they are not reduced by passing from NLO to NNLO. In Fig. 1, the KKSS  $b \rightarrow B$  FF [18] is included for comparison. It somewhat undershoots our NLO  $b \rightarrow B$  FF, which we attribute to the impact of the DELPHI data [22], which were not available at the time of the analysis in Ref. [18].

In Fig. 2(a), the analysis of Fig. 1 is repeated for  $\mu_F = M_Z$ , the c.m. energy of the experimental data fitted to. Our NLO and NNLO  $b \rightarrow B$  FFs are now closer together, the remaining difference being entirely due to the  $\mathcal{O}(\alpha_s^2)$  corrections to the hard-scattering cross sections. On the other hand, the difference between the NLO  $b \rightarrow B$  FF and the KKSS one is hardly affected by the DGLAP evolution from  $\mu_0$  to  $M_Z$ , as it is due to a difference in the collection of experimental data fitted to. Figure 2(b) is the counterpart of Fig. 2(a) for the  $g \rightarrow B$  FF, which is generated by DGLAP evolution from the initial condition

TABLE II. Values of the fit parameters in Eq. (4) obtained at NLO and NNLO.

Order	$N_b$	$\alpha_b$	$\beta_b$
NLO	2575.014	15.424	2.394
NNLO	1805.896	14.168	2.341

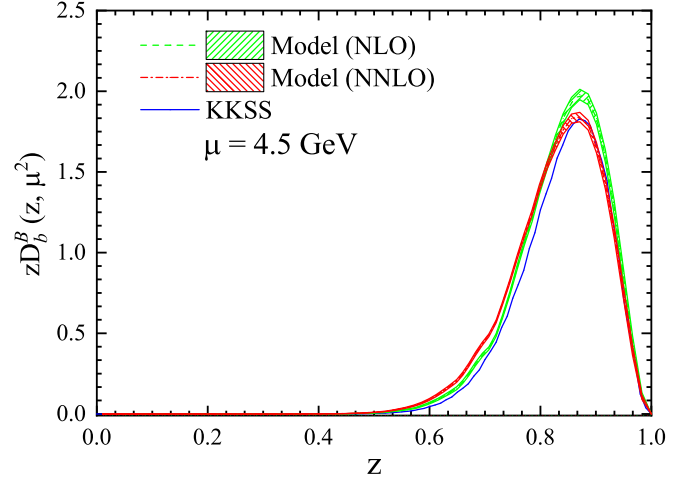


FIG. 1. Line shapes of  $zD_b^B(z, \mu_0)$  with  $\mu_0 = 4.5$  GeV at NLO (green dashed line) and NNLO (red dot-dashed line) and their experimental uncertainty bands (green and red hatched areas). The KKSS result [18] (blue solid line) is shown for comparison.

$D_g^B(z, \mu_0) = 0$ , as explained in Sec. II. Our NLO and NNLO results are now very similar; the KKSS result again falls below our NLO result. The comparisons between our NLO and NNLO results for the  $b \rightarrow B$  and  $g \rightarrow B$  FFs are refined in Figs. 2(c) and 2(d), respectively, where these FFs and their error bands are normalized with respect to the central values at NLO. Deviations occur at small and large values of  $z$ , which are outside the focus of our present study. They are due to large soft-gluon and threshold logarithms, respectively, which are included through  $\mathcal{O}(\alpha_s^2)$  at NNLO, but only to  $\mathcal{O}(\alpha_s)$  at NLO. These logarithms invalidate the fixed-order treatment at small and large values of  $z$  and should be resummed. This is, however, beyond the scope of our present analysis and left for future work.

In Fig. 3, the NLO and NNLO results for  $(1/\sigma_{\text{tot}})d\sigma(e^+e^- \rightarrow B + X)/dx_B$  evaluated with our respective  $B$ -hadron FF sets are compared with the experimental data fitted to. The uncertainty bands stem from those of the  $B$ -hadron FFs and are of experimental origin. We observe that the experimental data are in good mutual agreement and are well described both by the NLO and NNLO results down to  $x_B$  values of 0.4, say, as for both line shape and normalization. The NNLO description does somewhat better at lower values of  $x_B$ , which explains the lower value of  $\chi_{\text{global}}^2(p)/\text{DOF}$  in Table I. The failure of the theoretical descriptions in the small- $x_B$  regime is, of course, a direct consequence of the small- $x_B$  cuts applied.

For better visibility, we present the information contained in Fig. 3 as data over theory plots in Fig. 4, one for each experiment. Specifically, the experimental data are in turn normalized to the NLO and NNLO central values. As already explained above, the NLO and NNLO uncertainty bands are very similar. As already visible in Fig. 3, the

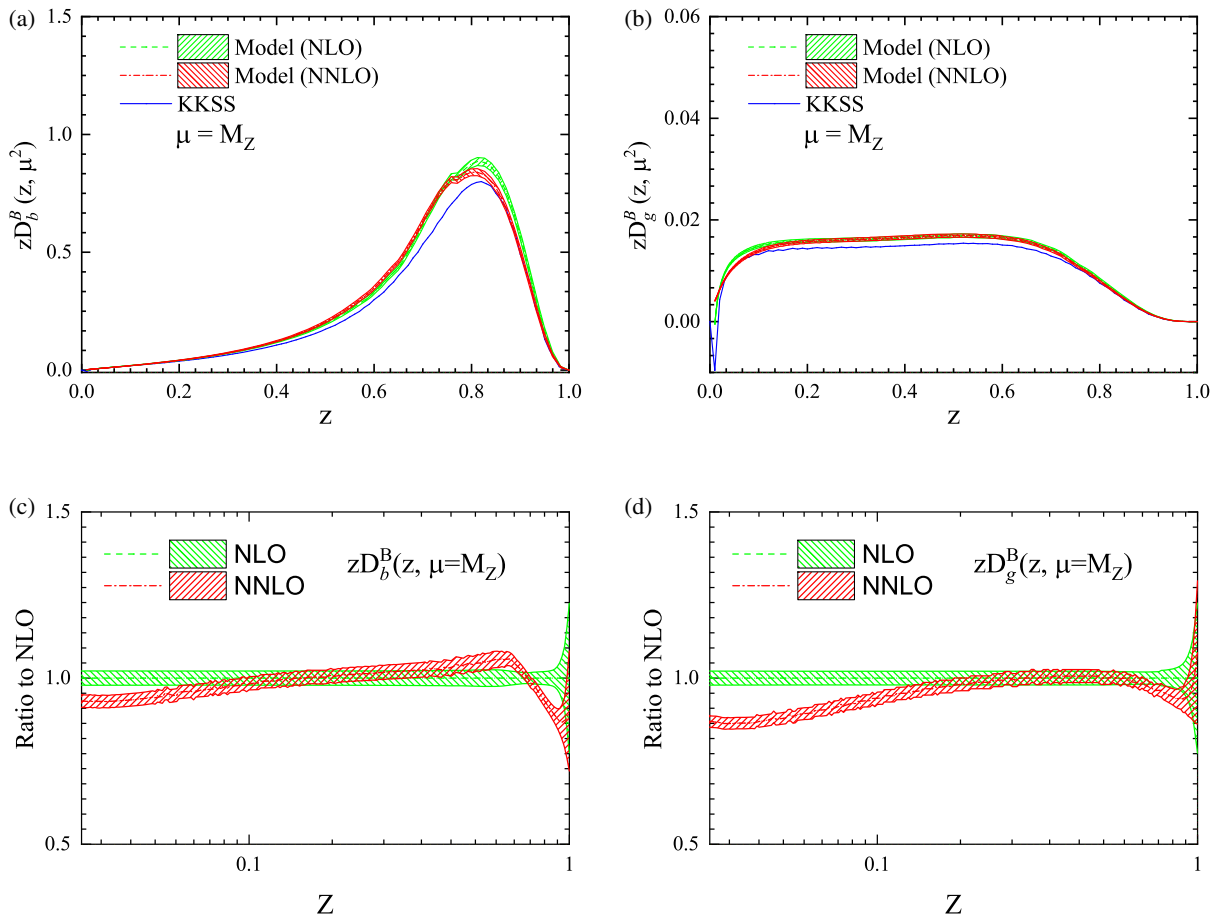


FIG. 2. Line shapes of (a)  $zD_b^B(z, M_Z)$  and (b)  $zD_g^B(z, M_Z)$  at NLO (green dashed lines) and NNLO (red dot-dashed lines) and their experimental uncertainty bands (green and red hatched areas). The KKSS results [18] (blue solid lines) are shown for comparison. NLO and NNLO results for (c)  $zD_b^B(z, M_Z)$  and (d)  $zD_g^B(z, M_Z)$  normalized with respect to the NLO central values.

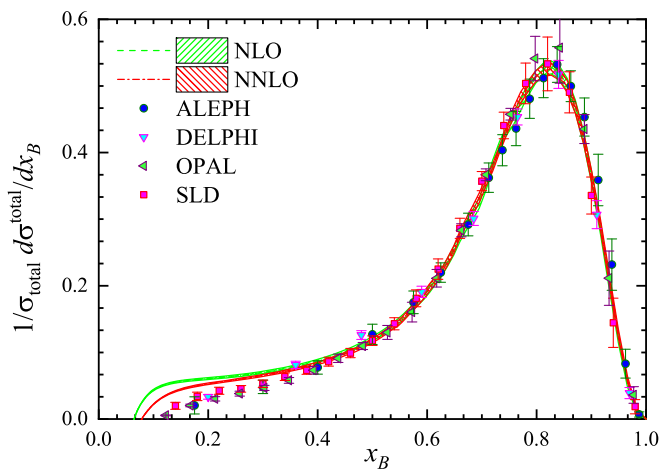


FIG. 3. The NLO (green dashed line) and NNLO (red dot-dashed line) results for  $(1/\sigma_{\text{total}})d\sigma(e^+e^- \rightarrow B + X)/dx_B$  evaluated with our respective  $B$ -hadron FF sets are compared with the experimental data fitted to, from ALEPH [19], DELPHI [22], OPAL [20], and SLD [21]. The uncertainty bands (green and red hatched areas) stem from those of the  $B$ -hadron FFs.

experimental data consistently undershoot the NLO and NNLO results in the small- $x_B$  regime. On the other hand, their large- $x_B$  behavior is nonuniform. While the ALEPH and OPAL data overshoot the NLO and NNLO results in the upper  $x_B$  range, there is nice agreement for the DELPHI and SLD data.

### V. B-HADRON PRODUCTION BY TOP-QUARK DECAY

As a topical application of our  $B$ -hadron FFs, we study inclusive single  $B$ -hadron production at the LHC.  $B$  hadrons may be produced directly or through the decay of heavier particles, including the  $Z$  boson, the Higgs boson, and the top quark. For definiteness, we concentrate here on the latter process,  $t \rightarrow BW^+ + X$ , where  $X$  collectively denotes any other final-state particles. This allows one to study properties of the top quark, such as its degree of polarization in a given production mode, which includes single and pair production. We thus consider both unpolarized and polarized top quarks.

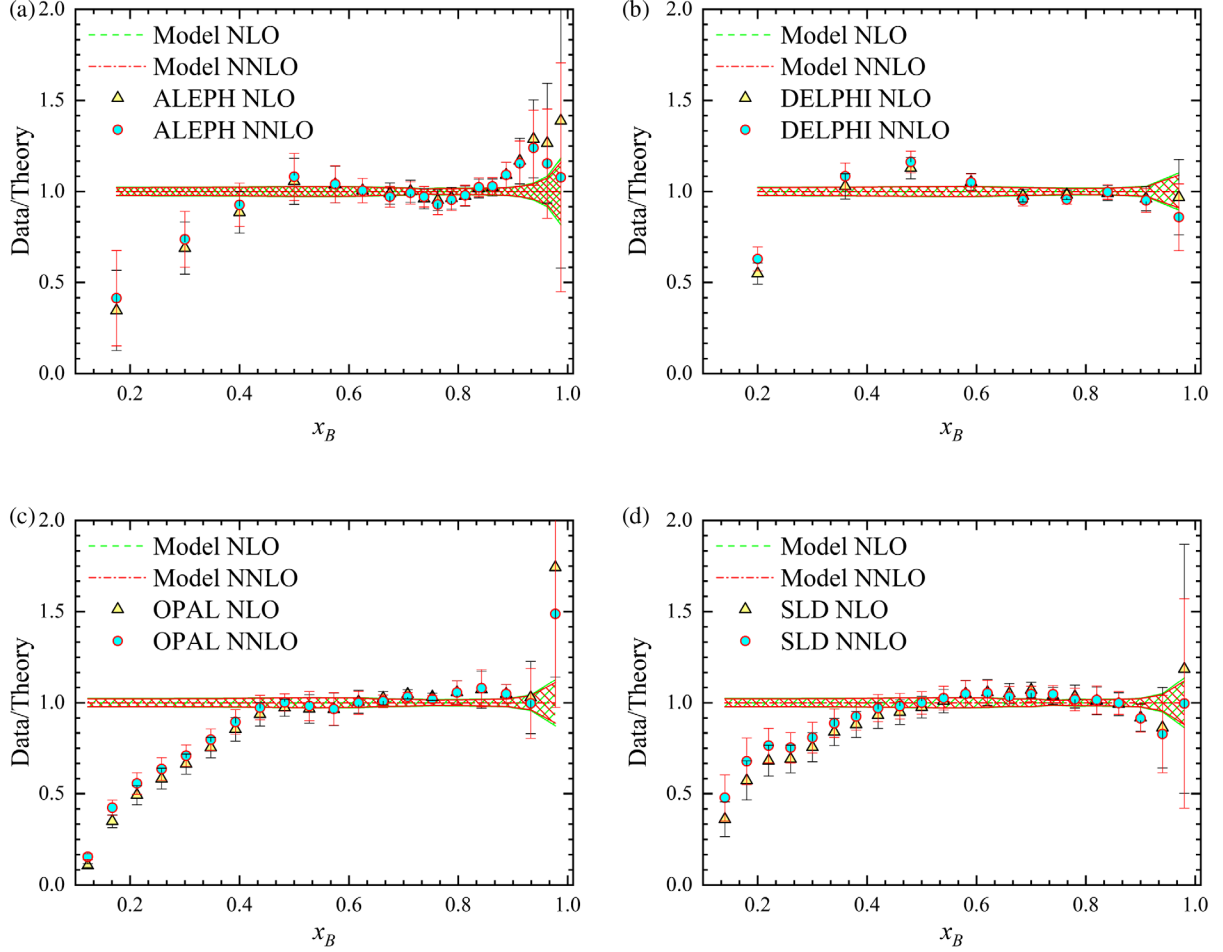


FIG. 4. (a) ALEPH [19], (b) DELPHI [22], (c) OPAL [20], and (d) SLD [21] data of  $(1/\sigma_{\text{tot}})d\sigma(e^+e^- \rightarrow B + X)/dx_B$  normalized with respect to our NLO (green hatched bands) and NNLO (red hatched bands) results.

We work in the rest frame of the top quark. The partial width of the decay  $t \rightarrow BW^+ + X$ , differential in the scaled  $B$ -hadron energy  $x_B$  and the angle  $\theta_P$  enclosed between the top-quark polarization three-vector  $\vec{P}$  and the  $B$ -hadron three-momentum  $\vec{p}_B$  is given by

$$\begin{aligned} \frac{d^2\Gamma}{dx_B d\cos\theta_P}(t \rightarrow BW^+ + X) \\ = \frac{1}{2} \left( \frac{d\Gamma^{\text{unpol}}}{dx_B} + P \frac{d\Gamma^{\text{pol}}}{dx_B} \cos\theta_P \right), \end{aligned} \quad (8)$$

where  $P = |\vec{P}|$  is the degree of polarization. In the ZM-VFNS, we have

$$\begin{aligned} \frac{d\Gamma^{\text{unpol/pol}}}{dx_B} = \sum_{i=b,g} \int_{x_i^{\min}}^{x_i^{\max}} \frac{dx_i}{x_i} \\ \times \frac{d\Gamma_i^{\text{unpol/pol}}}{dx_i}(x_i, \mu_R, \mu_F) D_i^B\left(\frac{x_B}{x_i}, \mu_F\right), \end{aligned} \quad (9)$$

where  $d\Gamma_i^{\text{unpol}}/dx_i$  and  $d\Gamma_i^{\text{pol}}/dx_i$  refer to the parton-level decay  $t \rightarrow iW^+ + X$ , differential in the scaled energy  $x_i$  of parton  $i = b, g$ . In the top-quark rest frame, we have  $x_B = E_B/E_b^{\max}$  and  $x_i = E_i/E_b^{\max}$ , where  $E_B$  and  $E_i$  are the energies of the  $B$  hadron and parton  $i$ , and  $E_b^{\max}$  is the maximum energy of the bottom quark. In our application of the ZM-VFNS, where  $m_b \ll \mu_F = \mathcal{O}(m_t)$ , the bottom quark is taken to be massless. By the same token, we also neglect the  $B$ -hadron mass  $m_B$ . So far,  $d\Gamma_i^{\text{unpol}}/dx_i$  and  $d\Gamma_i^{\text{pol}}/dx_i$  are only available through NLO; analytic expressions may be found in Refs. [32–34] and Refs. [35–38], respectively. In Ref. [38],  $\theta_P$  is taken to be enclosed between  $\vec{P}$  and the  $W$ -boson three-momentum  $\vec{p}_W$ . Although a consistent analysis is presently limited to NLO, we also employ our NNLO  $B$ -hadron FF set to explore the possible size of the NNLO corrections.

In our numerical analysis, we use  $m_b = 4.5$  GeV,  $m_W = 80.379$  GeV, and  $m_t = 173.0$  GeV [26], and choose  $\mu_R = \mu_F = m_t$ . In Fig. 5(a), we present the NLO predictions of  $d\Gamma^{\text{unpol}}/dx_B$  and  $d\Gamma^{\text{pol}}/dx_B$ , evaluated with our NLO  $B$ -hadron FF set. For comparison, the evaluations

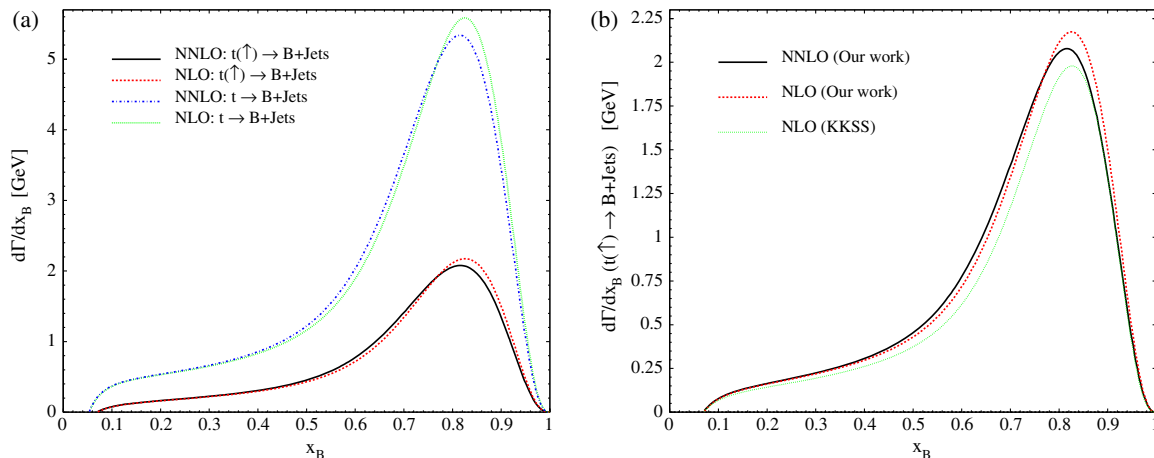


FIG. 5. (a) NLO predictions of  $d\Gamma^{\text{unpol}}/dx_B$  (green dotted line) and  $d\Gamma^{\text{pol}}/dx_B$  (red dashed line), evaluated with our NLO  $B$ -hadron FF set. For comparison, the evaluations with our NNLO  $B$ -hadron FF set are also included (blue dot-dashed and black solid lines). (b) The results for  $d\Gamma^{\text{pol}}/dx_B$  in Fig. 5(a) are compared to the evaluation with the KKSS  $B$ -hadron FF set [18] (green dotted line).

with our NNLO  $B$ -hadron FF set are also included. We observe from Fig. 5(a) that switching from the NLO  $B$ -hadron FF set to the NNLO one slightly smoothens the theoretical prediction, decreasing it in the peak region and increasing it in the tail region thereunder. At the same time, the peak position is shifted towards smaller values of  $x_B$ . The change in normalization is of order 5% at most. These effects should mark an upper limit of the total NNLO corrections because the as-yet-unknown NNLO corrections to  $d\Gamma_i^{\text{unpol}}/dx_i$  and  $d\Gamma_i^{\text{pol}}/dx_i$  are expected to give rise to some compensation if FF universality is realized in nature. In Fig. 5(b), the results for  $d\Gamma^{\text{pol}}/dx_B$  in Fig. 5(a) are compared to the evaluation with the KKSS  $B$ -hadron FF set [18]. As in Figs. 1, 2(a), and 2(b), the NLO result is somewhat reduced by switching to the KKSS  $B$ -hadron FF set.

## VI. SUMMARY AND CONCLUSIONS

In this paper, we determined nonperturbative FFs for  $B$  hadrons, both at NLO and NNLO in the ZM-VFNS, by fitting to all available experimental data of inclusive single  $B$ -hadron production in  $e^+e^-$  annihilation,  $e^+e^- \rightarrow B + X$ , from ALEPH [19], DELPHI [22], OPAL [20], and SLD [21]. We then applied these  $B$ -hadron FFs to provide NLO predictions for inclusive  $B$ -hadron production by top-quark decay,  $t \rightarrow BW^+ + X$ , both for unpolarized and polarized top quarks.

Our analysis updates and improves similar ones in the literature [17,18] in the following respects. We included the DELPHI data [22], which had not been available then. For the first time, we advanced to NNLO in a fit of  $B$ -hadron FFs. We performed a careful estimation of the experimental uncertainties in our  $B$ -hadron FFs using the Hessian approach.

We adopted the simple power ansatz of Eq. (4) and obtained for the three fit parameters appearing therein the values listed in Table II. The goodness of the NLO and NNLO fits turned out to be excellent, with  $\chi^2/\text{DOF}$  values of 1.485 and 1.104, respectively (see Table I). As expected on general grounds, the fit quality is improved by ascending to higher orders of perturbation theory.

We encourage the LHC collaborations to measure the  $x_B$  distribution of the partial width of the decay  $t \rightarrow BW^+ + X$ , for two reasons. On the one hand, this will allow for an independent determination of the  $B$ -hadron FFs and thus provide a unique chance to test their universality and DGLAP scaling violations, two important pillars of the parton model of QCD. On the other hand, this will allow for a determination of the top-quark polarization, which should depend on the production mode.

The theoretical framework provided by the ZM-VFNS was quite appropriate for the present analysis, since the characteristic energy scales of the considered processes,  $M_Z$  and  $m_t$ , greatly exceeded the bottom-quark mass  $m_b$ , which could thus be neglected. Possible theoretical improvements include the inclusion of finite- $m_b$  and finite- $m_B$  effects, and the resummation of soft-gluon logarithms, which extend the validity towards small values of  $x_B$ , and the resummation of threshold logarithms, which extends the validity towards large values of  $x_B$ . The general-mass variable-flavor-number scheme (GM-VFNS) [39–42] provides a consistent and natural finite- $m_b$  generalization of the ZM-VFNS on the basis of the  $\overline{\text{MS}}$  factorization scheme [43]. The processes considered here,  $e^+e^- \rightarrow B + X$  [44],  $t \rightarrow BW^+ + X$  [34], and  $t(\uparrow) \rightarrow BW^+ + X$  [45], have all been worked out in the GM-VFNS at NLO, but not yet at NNLO. Finite- $m_b$  effects may be conveniently incorporated using the approach of Refs. [46–48]. The implementation of such theoretical improvements

reaches beyond the scope of the present analysis and is left for future work.

### ACKNOWLEDGMENTS

Hamzeh Khanpour and Maryam Soleymaninia thank the School of Particles and Accelerators at the Institute for

Research in Fundamental Sciences (IPM) for financial support. Hamzeh Khanpour is also grateful to the University of Science and Technology of Mazandaran for financial support. This work was supported in part by the German Federal Ministry for Education and Research (BMBF) through Grant No. 05H18GUCC1.

- 
- [1] C. Albajar *et al.* (UA1 Collaboration), *Phys. Lett. B* **213**, 405 (1988).
- [2] V. N. Gribov and L. N. Lipatov, *Yad. Fiz.* **15**, 781 (1972) [*Sov. J. Nucl. Phys.* **15**, 438 (1972)].
- [3] G. Altarelli and G. Parisi, *Nucl. Phys.* **B126**, 298 (1977).
- [4] Y. L. Dokshitzer, *Zh. Eksp. Teor. Fiz.* **73**, 1216 (1977) [*Sov. Phys. JETP* **46**, 641 (1977)].
- [5] A. Mitov, S. Moch, and A. Vogt, *Phys. Lett. B* **638**, 61 (2006).
- [6] S. Moch and A. Vogt, *Phys. Lett. B* **659**, 290 (2008).
- [7] A. A. Almasy, S. Moch, and A. Vogt, *Nucl. Phys.* **B854**, 133 (2012).
- [8] P. J. Rijken and W. L. van Neerven, *Phys. Lett. B* **386**, 422 (1996).
- [9] P. J. Rijken and W. L. van Neerven, *Phys. Lett. B* **392**, 207 (1997).
- [10] P. J. Rijken and W. L. van Neerven, *Nucl. Phys.* **B487**, 233 (1997).
- [11] A. Mitov and S. Moch, *Nucl. Phys.* **B751**, 18 (2006).
- [12] D. P. Anderle, M. Stratmann, and F. Ringer, *Phys. Rev. D* **92**, 114017 (2015).
- [13] V. Bertone, S. Carrazza, N. P. Hartland, E. R. Nocera, and J. Rojo (NNPDF Collaboration), *Eur. Phys. J. C* **77**, 516 (2017).
- [14] M. Soleymaninia, M. Goharipour, and H. Khanpour, *Phys. Rev. D* **98**, 074002 (2018).
- [15] M. Soleymaninia, M. Goharipour, and H. Khanpour, *Phys. Rev. D* **99**, 034024 (2019).
- [16] M. Soleymaninia, H. Khanpour, and S. M. Moosavi Nejad, *Phys. Rev. D* **97**, 074014 (2018).
- [17] J. Binnewies, B. A. Kniehl, and G. Kramer, *Phys. Rev. D* **58**, 034016 (1998).
- [18] B. A. Kniehl, G. Kramer, I. Schienbein, and H. Spiesberger, *Phys. Rev. D* **77**, 014011 (2008).
- [19] A. Heister *et al.* (ALEPH Collaboration), *Phys. Lett. B* **512**, 30 (2001).
- [20] G. Abbiendi *et al.* (OPAL Collaboration), *Eur. Phys. J. C* **29**, 463 (2003).
- [21] K. Abe *et al.* (SLD Collaboration), *Phys. Rev. D* **65**, 092006 (2002); **66**, 079905(E) (2002).
- [22] J. Abdallah *et al.* (DELPHI Collaboration), *Eur. Phys. J. C* **71**, 1557 (2011).
- [23] J. Pumplin, D. R. Stump, and W. K. Tung, *Phys. Rev. D* **65**, 014011 (2001).
- [24] K. G. Chetyrkin, A. L. Kataev, and F. V. Tkachov, *Phys. Lett.* **85B**, 277 (1979).
- [25] V. G. Kartvelishvili and A. K. Likhoded, *Yad. Fiz.* **42**, 1306 (1985) [*Sov. J. Nucl. Phys.* **42**, 823 (1985)].
- [26] M. Tanabashi *et al.* (Particle Data Group), *Phys. Rev. D* **98**, 030001 (2018).
- [27] D. Stump, J. Pumplin, R. Brock, D. Casey, J. Huston, J. Kalk, H. L. Lai, and W. K. Tung, *Phys. Rev. D* **65**, 014012 (2001).
- [28] J. Blümlein, H. Böttcher, and A. Guffanti, *Nucl. Phys.* **B774**, 182 (2007).
- [29] F. James and M. Roos, *Comput. Phys. Commun.* **10**, 343 (1975).
- [30] V. Bertone, S. Carrazza, and J. Rojo, *Comput. Phys. Commun.* **185**, 1647 (2014).
- [31] A. D. Martin, W. J. Stirling, R. S. Thorne, and G. Watt, *Eur. Phys. J. C* **63**, 189 (2009).
- [32] G. Corcella and A. D. Mitov, *Nucl. Phys.* **B623**, 247 (2002).
- [33] M. Cacciari, G. Corcella, and A. D. Mitov, *J. High Energy Phys.* **12** (2002) 015.
- [34] B. A. Kniehl, G. Kramer, and S. M. Moosavi Nejad, *Nucl. Phys.* **B862**, 720 (2012).
- [35] M. Fischer, S. Groote, J. G. Korner, M. C. Mauser, and B. Lampe, *Phys. Lett. B* **451**, 406 (1999).
- [36] M. Fischer, S. Groote, J. G. Korner, and M. C. Mauser, *Phys. Rev. D* **65**, 054036 (2002).
- [37] S. M. Moosavi Nejad, *Phys. Rev. D* **88**, 094011 (2013).
- [38] S. M. Moosavi Nejad and M. Balali, *Phys. Rev. D* **90**, 114017 (2014); **93**, 119904(E) (2016).
- [39] G. Kramer and H. Spiesberger, *Eur. Phys. J. C* **22**, 289 (2001), <https://link.springer.com/article/10.1007/s100520100805>.
- [40] B. A. Kniehl, G. Kramer, I. Schienbein, and H. Spiesberger, *Phys. Rev. D* **71**, 014018 (2005).
- [41] B. A. Kniehl, G. Kramer, I. Schienbein, and H. Spiesberger, *Eur. Phys. J. C* **41**, 199 (2005).
- [42] B. A. Kniehl, G. Kramer, I. Schienbein, and H. Spiesberger, *Phys. Rev. Lett.* **96**, 012001 (2006).
- [43] J. C. Collins, *Phys. Rev. D* **58**, 094002 (1998).
- [44] T. Kneesch, B. A. Kniehl, G. Kramer, and I. Schienbein, *Nucl. Phys.* **B799**, 34 (2008).
- [45] S. M. Moosavi Nejad and M. Balali, *Eur. Phys. J. C* **76**, 173 (2016).
- [46] S. Albino, B. A. Kniehl, G. Kramer, and W. Ochs, *Phys. Rev. D* **73**, 054020 (2006).
- [47] S. Albino, B. A. Kniehl, G. Kramer, and C. Sandoval, *Phys. Rev. D* **75**, 034018 (2007).
- [48] S. Albino, B. A. Kniehl, and G. Kramer, *Nucl. Phys.* **B803**, 42 (2008).